



Apertureless near-field microscopy using a knife blade as a scanning probe at millimeter wavelengths

Tatsuo Nozokido, Manabu Ishino, Masakazu Tokuriki, Hiroyuki Kamikawa, and Jongsuck Bae

Citation: [Journal of Applied Physics](#) **112**, 074907 (2012); doi: 10.1063/1.4757954

View online: <http://dx.doi.org/10.1063/1.4757954>

View Table of Contents: <http://scitation.aip.org/content/aip/journal/jap/112/7?ver=pdfcov>

Published by the [AIP Publishing](#)



Re-register for Table of Content Alerts

Create a profile.



Sign up today!



Apertureless near-field microscopy using a knife blade as a scanning probe at millimeter wavelengths

Tatsuo Nozokido,^{1,a)} Manabu Ishino,¹ Masakazu Tokuriki,¹ Hiroyuki Kamikawa,¹ and Jongsuck Bae²

¹Graduate School of Science and Engineering for Research, University of Toyama, 3190 Gofuku, Toyama 930-8555, Japan

²Department of Engineering Physics, Electronics, and Mechanics, Nagoya Institute of Technology, Gokiso, Showa-ku, Nagoya 466-8555, Japan

(Received 25 June 2012; accepted 10 September 2012; published online 5 October 2012)

We report on the use of a knife blade as a scanning probe for apertureless near-field microscopy at millimeter wavelengths. Since the knife blade probe is a wider version of the metal tip probe commonly used in this technique, and therefore the interaction area between the probe tip and the sample is larger, an improvement in the intensity of the measured near-field signal is expected. The knife blade probe can also work as a part of a resonator in the illumination optics used in this microscopy format to enhance the strength of the near field that interacts with the sample, resulting in a further improvement in the signal intensity. A scanning method and an image reconstruction algorithm based on computerized tomography are adopted to obtain 2-D near-field images. Experiments performed at 60 GHz using a knife blade with a tip radius of $6\ \mu\text{m}$ ($\sim\lambda/1000$) show that the signal intensity is enhanced by ~ 20 dB compared with an equivalent metal tip probe, and that an image resolution approaching the tip radius of the knife blade is achieved. © 2012 American Institute of Physics. [<http://dx.doi.org/10.1063/1.4757954>]

I. INTRODUCTION

The scanning near-field imaging technique has been utilized in a variety of instruments that cover frequencies spanning the microwave-to-optical regions. Many kinds of near-field probes have been proposed and used during the development of the technique, because they determine the image resolution and sensitivity attainable in scanning near-field microscopy.¹ In the microwave region, coaxial probes^{2–9} are the ones most commonly used. These probes are made up of a fine coaxial cable with a sharpened central conductor protruding from the outer shielding. The spatial resolution is determined by the size of the tip of the inner conductor. Microstrip- and strip-lines, and a small aperture in a conducting screen are also used as near-field probes in the microwave region.^{10–12} In the millimeter-wave region, tapered dielectric waveguides are used.^{13,14} Slit-type probes^{15–21} featuring no cutoff, having a slit-like aperture in a rectangular or a parallel plate waveguide, are suitable for use in the millimeter and terahertz wave regions because of the simplicity of their structure. In comparison with optical waves, the benefit of using radio waves such as microwaves, millimeter waves, and terahertz waves in scanning near-field microscopy lies in the promise of new types of material contrast. A good example is the mapping of electronic transport properties in semiconductors and in biological systems.^{16,22–24}

At higher frequencies than millimeter waves, especially in the terahertz and infrared regions, possibly due to the lack of low-loss waveguides, a sharp metal tip is widely

used as a scanning probe.^{23,25–35} In this microscopy format, the metal tip is held close to the surface of the sample and evanescent waves are converted to propagating waves. The radiation scattered from the incident radiation is measured for imaging. This technique is called apertureless near-field microscopy, since apertures to confine the incident radiation or limit the collection area are not used. As is the case for the coaxial probe, the spatial resolution is determined by the radius of curvature of the tip. The metal tip probes are easy to fabricate and permit extreme subwavelength resolution because of the simplicity of their structure. The signal intensity of the scattered waves, however, is relatively so small that it is submerged within a large background signal.

We report here the use of a knife blade as a scanning probe for apertureless near-field microscopy to demonstrate the enhancement of the signal intensity and 2-D image reconstruction at millimeter wavelengths. Since the knife blade is wider than the metal tip, and hence the interaction area between the tip and the sample is larger, an improvement in the signal intensity of the scattered waves is expected. Because the width of the knife blade can be larger than the diffraction-limited spot size of the incident radiation, further improvement can also be expected when incorporating a resonator in the illumination optics using the knife blade as part of the resonator to enhance the strength of the near field interacting with the sample. Although the experiments were carried out at a millimeter-wave frequency of 60 GHz, the apertureless near-field scanning microscopy using a knife blade investigated here can also be implemented in the terahertz and infrared regions to improve the signal-to-noise ratio in image acquisition.

^{a)}Electronic mail: nozokido@eng.u-toyama.ac.jp.

II. EXPERIMENTAL SETUP

Fig. 1 is a schematic drawing of our millimeter-wave apertureless near-field scanning microscope using a knife blade. Radiation at 60 GHz ($\lambda = 5$ mm) from a circular horn antenna having an aperture diameter of 10 mm is incident on the knife blade probe with p -polarization. The distance between the aperture of the circular horn antenna and the probe tip is 8 mm. Scattered waves from the probe are collected by a 100-mm-diameter polyethylene lens having a focal length of 72 mm and then received by a standard-gain rectangular horn antenna. The distance between the aperture of the rectangular horn antenna and the lens, and that between the lens and the probe tip are 60 mm and 124 mm, respectively. The acceptance angle of the receiver θ_a is 20° . Both antennas are connected to waveguide-to-coaxial transformers (not shown in Fig. 1) that are connected via coaxial cables to a vector network analyzer (VNA: Agilent 8510C) to measure the complex transmission coefficient from port 1 to port 2, S_{21} . The total transmission ($|S_{21}| = 1$ Unit) was calibrated by directly connecting both transformers. The sample to be imaged is placed on a sample mount consisting of a hemispherical glass lens and an antireflection layer.¹⁷ The probe-to-sample separation is adjusted between Z_L and Z_U , as depicted in the inset of Fig. 1, by a piezoelectric transducer (PZT) and a laser displacement sensor.

A scanning method and an image reconstruction algorithm based on computerized tomography for 2-D image reconstruction^{16–18} are used in order to facilitate deconvolution of the tip shape of the knife blade. The sample to be imaged is scanned linearly for different sample-rotation angles by a scanner using linear and rotational motor-driven stages. A PC controls the scanner and the PZT, saves raw data collected as projections from the VNA, and also executes image reconstruction by a filtered back-projection (FBP) algorithm.³⁶ Since the raw data acquired are complex numbers, intensity

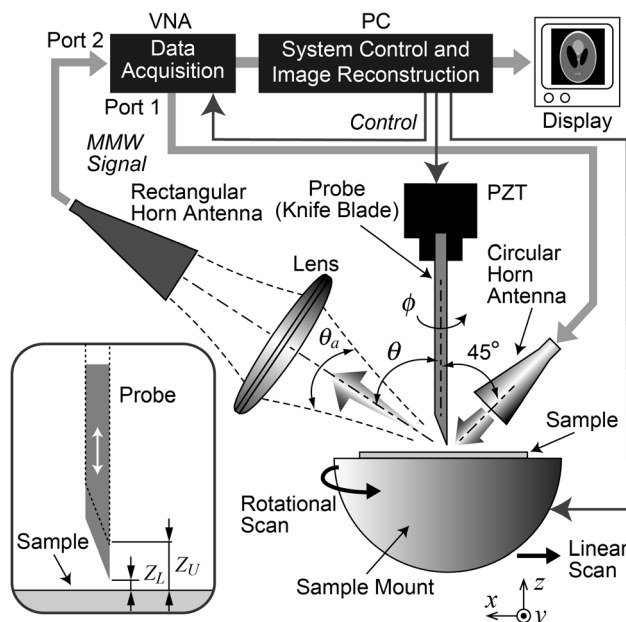


FIG. 1. Experimental setup for apertureless near-field scanning microscopy using a knife blade at millimeter wavelengths.

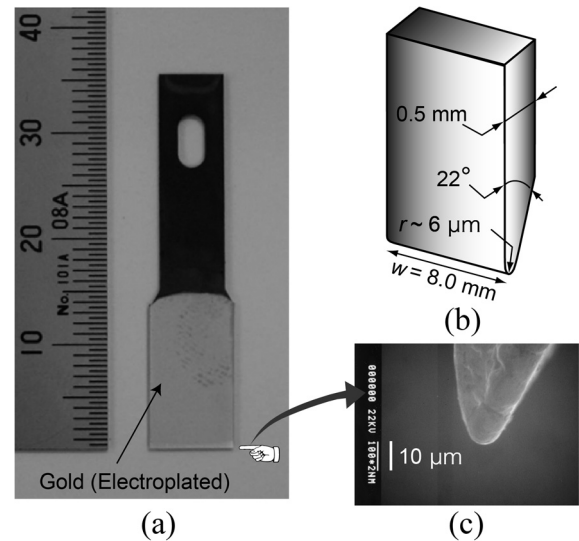


FIG. 2. Knife blade used as a scanning probe for apertureless near-field microscopy. (a) Photograph. (b) Dimensions of the probe. (c) Scanning electron micrograph of the tip.

and phase images are obtained after image reconstruction. For each of the scanning points, two values of S_{21} at different tip-to-sample separations, Z_L and Z_U , are acquired and the vectorial difference between them ΔS_{21} is calculated and recorded in order to extract pure near-field information by eliminating unwanted background signals caused by surface waves within the sample, reflected waves from outside the imaging area, and so on. Z_L and Z_U were set as $1 \mu\text{m}$ and $7 \mu\text{m}$, respectively, in all the experiments.

For this proof-of-concept experiment for 2-D image reconstruction using a knife blade probe, a commercially available knife made of stainless steel (OLFA Art knife XB157H) was selected for use as the near-field probe. The knife was cleaned and then electroplated with gold (Au) to produce a good scatterer. Figs. 2(a)–2(c) show a photograph of the completed probe, its dimensions, and a scanning electron micrograph of the probe tip, respectively. The width of the probe is 8 mm (1.6λ) and the radius of curvature of the edge, i.e., the tip, is $6 \mu\text{m}$ ($\sim \lambda/1000$). For perfect image reconstruction to retrieve the physical properties of the sample, the sample should be a planar substrate with the topographical variation of the surface much smaller than the tip radius of the knife blade.

III. RESULTS

A. Comparison of knife blade and metal tip probes

The near-field signal is affected by the antenna properties of the near-field probe. Since the near-field signal in apertureless near-field microscopy originates from the tip-sample interaction occurring in close proximity to the tip at the end of the probe, the metal tip and knife blade probes can be treated as antennas being excited at their tips. In this case, the metal tip is modeled as a long-wire antenna. The knife blade is a patch antenna with fringing electric fields responsible for radiation at one side of the patch. The radiation patterns of the near-field signals for the metal tip and the knife blade in spherical coordinates are³⁷

$$F_{\text{metal tip}}(\theta) = K \sin \theta \frac{\sin[(\pi L/\lambda)(1 - \cos \theta)]}{(\pi L/\lambda)(1 - \cos \theta)} \quad (1)$$

and

$$F_{\text{knife blade}}(\theta, \phi) = \frac{\sin[(\pi W/\lambda) \sin \theta \sin \phi]}{(\pi W/\lambda) \sin \theta \sin \phi}, \quad (2)$$

respectively, where L is the antenna length of the metal tip, K is a normalization constant that depends on the length L , W is the width of the knife blade, λ is the wavelength, θ is the polar angle measured from the z axis (axis of the probe), and ϕ is the azimuthal angle measured from the x axis (see Fig. 1). In the x - z ($\phi = 0^\circ$) and y - z ($\phi = 90^\circ$) planes, Eq. (2) reduces to

$$F_{\text{knife blade}}(\theta) = 1 \quad (3)$$

and

$$F_{\text{knife blade}}(\theta) = \frac{\sin[(\pi W/\lambda) \sin \theta]}{(\pi W/\lambda) \sin \theta}, \quad (4)$$

respectively. The above equations show that the radiation patterns of both probes are rotationally symmetric around the z axis for the metal tip and around the y axis for the knife blade. Fig. 3 compares the radiation properties of both probes. Antenna gains and beam widths (FWHM) are calculated from Eqs. (1) and (4) as functions of the antenna length L of the metal tip and the width W of the knife blade normalized by the wavelength λ . For both probes, as the length and the width get larger, the gains increase. When the normalized antenna length and the width are smaller than 1.6, the gain of the metal tip is larger than that of the knife blade, while if these dimensions are larger than 1.6, the gain of the knife blade is larger due to more sidelobes arising in the case of the metal tip than the knife blade. When comparing the intensities of the near-field signal for each probe using the same receiver, a fair comparison can be made using near-field probes with the same radiation properties. This is the reason for selecting a knife blade with a width of 8 mm (1.6λ) for the experiments.

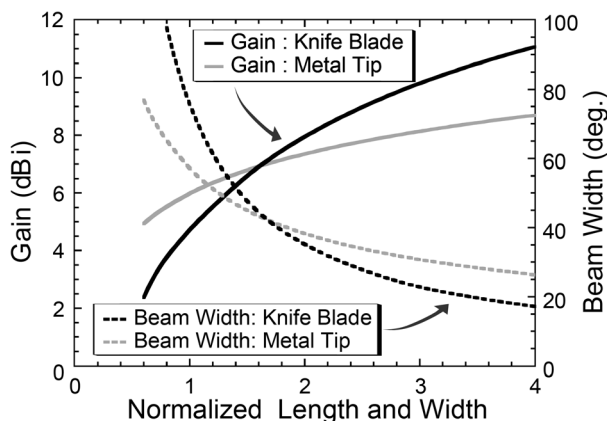


FIG. 3. Radiation properties of the metal tip and knife blade probes as antennas.

Fig. 4 compares the intensities of the near-field signal $|\Delta S_{21}|$ as a function of the receiver angle θ for the knife blade and metal tips with different antenna lengths of 4 mm and 8 mm. For the metal tip probes, a 0.3-mm-diameter tungsten wire was sharpened at one end by an electroetching technique and then electroplated with Au. The antenna length of the metal tip was defined by a right angle bend introduced into the wire at a designated distance from the tip. The radius of curvature of the tip is $7\ \mu\text{m}$, which is equivalent to that of the knife blade. The sample was a mirror-polished quartz substrate with a thickness of 0.5 mm and a diameter of 40 mm. The same quartz substrates were used for the other samples in the following. The angle of maximum radiation for the metal tip probe can be approximated by³⁷

$$\theta_{\text{max}} = \cos^{-1}\left(1 - 0.371(\lambda/L)\right). \quad (5)$$

For the metal tip probes with antenna lengths of 4 and 8 mm, these angles are calculated from Eq. (5) to be 58° and 40° , respectively, which agree well with the experimental results. The intensity of the near-field signal obtained using the knife blade probe is nearly constant within the measured range of θ , as expected from Eq. (3).

Fig. 5 compares one-dimensional scans of aluminum (Al) dots patterned on a quartz substrate for the knife blade probe and the metal tip probe with the 8-mm-long antenna. The thickness of the Al was $0.3\ \mu\text{m}$, which is one skin depth in Al at 60 GHz and is the same for the other patterned samples used in the experiments. The intensity $|\Delta S_{21}|$ and phase $\arg(\Delta S_{21})$ of the near-field signal ΔS_{21} were recorded. The scanning arrangement and a schematic diagram of the sample are depicted in Fig. 5(a). In this experiment, the receiver angles were optimized for each probe. The one-dimensional scans in Fig. 5(b) show that the signal level obtained using the knife blade is ~ 6 times (15.6 dB) greater than that using the metal tip, and that the contrast mechanism for these two types of probe is the same. It is also noticed that the random phase variation due to noise for the metal tip diminishes in the case of the knife blade.

B. 2-D near-field imaging using the knife blade probe

In order to reconstruct images correctly by the FBP algorithm when using the knife blade, the measured signal should

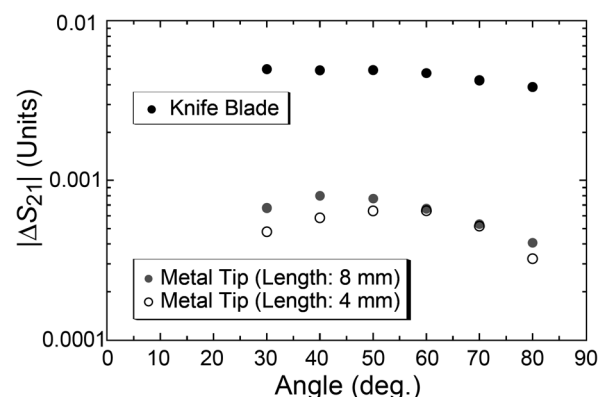


FIG. 4. Intensity of the near-field signal $|\Delta S_{21}|$ as a function of the receiver angle θ for the metal tip and the knife blade probes.

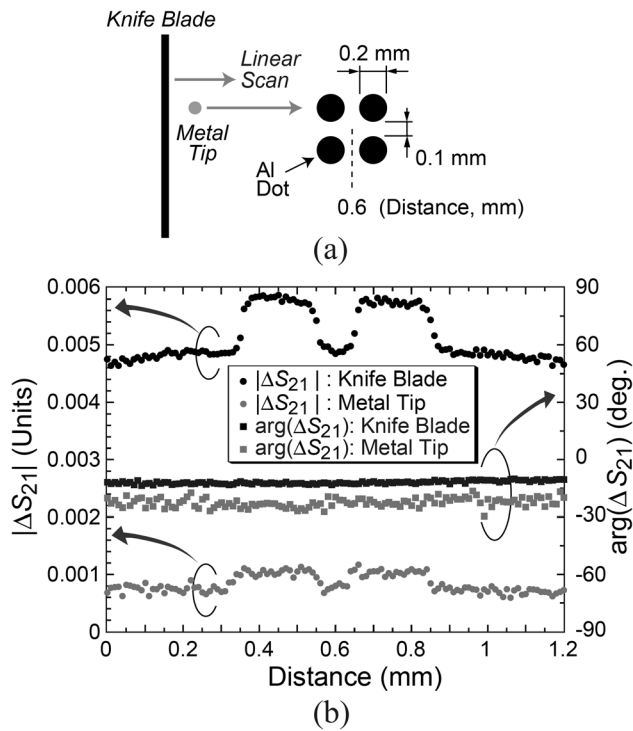


FIG. 5. One-dimensional scans of metal dots patterned on a quartz substrate for two kinds of near-field probe. (a) Schematic of the sample and scanning arrangement. (b) Intensity and phase variation of ΔS_{21} .

reflect the line integral of the physical properties of the sample along the width direction of the probe tip.^{16,36} To check this for the knife blade, metal lines with different lengths were taken as samples. Fig. 6 shows one-dimensional scans of Al

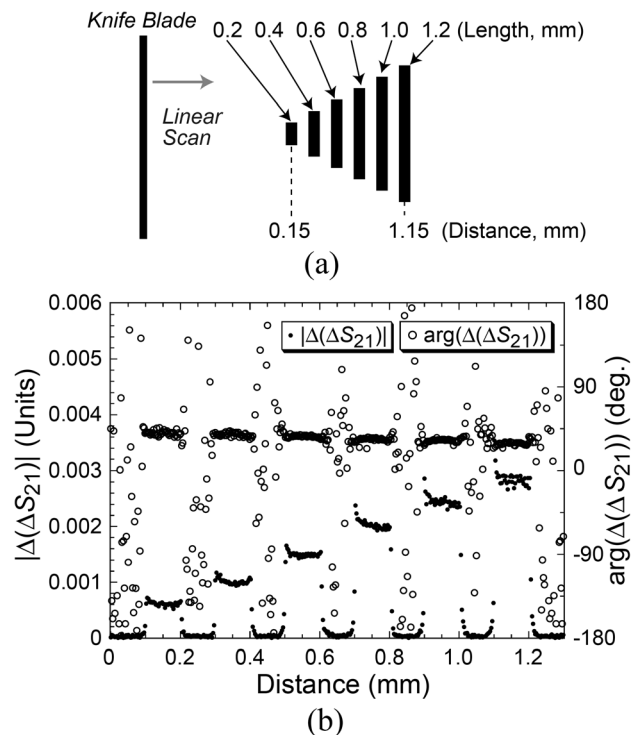


FIG. 6. One-dimensional scans of metal lines of different lengths using the knife blade probe. (a) Schematic of the sample and scanning arrangement. (b) Intensity and phase variation of $\Delta(\Delta S_{21})$.

lines patterned on a quartz substrate. The lengths of the lines vary from 0.2 to 1.2 mm, while their widths are all the same (0.1 mm). The step size (sampling interval) of the linear scan was $3 \mu\text{m}$. The measured data were processed in order to set the data for the quartz substrate such that $|\Delta S_{21}| = 0$ and $\arg(\Delta S_{21}) = 0$. This was done by subtracting the value of ΔS_{21} corresponding to the quartz substrate from each of the measured data in vectorial operations. The effect of this operation on the images reconstructed by the FBP algorithm is that the image intensity and phase corresponding to the quartz plate are set to zero. The resulting differences in intensity $|\Delta(\Delta S_{21})|$ and phase $\arg(\Delta(\Delta S_{21}))$ are plotted in Fig. 6(b). This result proves the validity of using the FBP algorithm for the knife blade to reconstruct 2-D images, since the intensity is proportional to the length of the metal lines, and the phase remains constant regardless of the length of the metal lines. This result also shows that deconvolution of the tip shape of the knife blade is possible, indicating that the image contrast of the reconstructed images by the FBP algorithm is identical to that of the image obtained using a metal tip. From the 10% to 90% rises and the 90% to 10% falls of the profile of $|\Delta(\Delta S_{21})|$, we estimated the spatial resolution of the knife blade to be $6.7 \mu\text{m}$, which is equivalent to the tip radius of the probe.

Reconstructed millimeter-wave images using the knife blade are shown in Fig. 7. The sample was the metal dots depicted in Fig. 5(a). Raw data sets for the images were obtained under experimental conditions in which the sampling interval for the linear scan was $10 \mu\text{m}$, the number of sampling points was 121, the angle interval for the rotational scan was 1.5° , and the total number of projections (linear

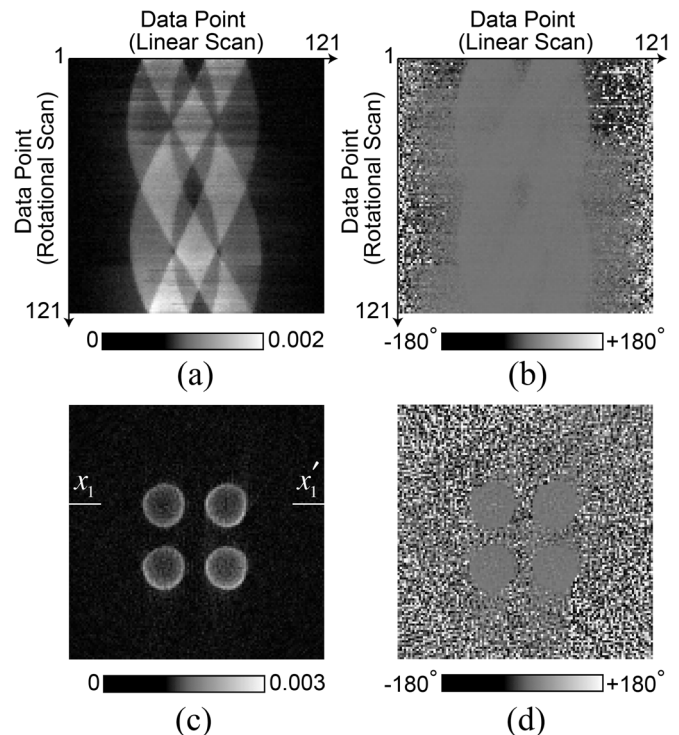


FIG. 7. Reconstructed millimeter-wave images of metal dots. (a) Intensity variation $|\Delta(\Delta S_{21})|$ of the raw data. (b) Phase variation $\arg(\Delta(\Delta S_{21}))$. (c) Reconstructed intensity image. (d) Reconstructed phase image.

scans) was 121. Figs. 7(a) and 7(b) show the differences in intensity $|\Delta(\Delta S_{21})|$ and phase $\arg(\Delta(\Delta S_{21}))$ of the raw data, respectively. These are displayed as gray scale images. Image reconstruction of the data in Figs. 7(a) and 7(b) was done using the FBP algorithm. Fig. 7(c) is the reconstructed millimeter-wave intensity image, and Fig. 7(d) is the phase image. The pixel values in the intensity image have the same units as the raw data, i.e., Units. The image size is $1.2 \text{ mm} \times 1.2 \text{ mm}$. These millimeter-wave images reflect fairly accurately the structure of the sample.

Since the knife blade and the sample form a corner reflector, further enhancement in the intensity of the near-field signal can be expected when a partial reflector is inserted in the incident beam path in order to incorporate a resonator comprising the partial reflector and the corner reflector in the illumination optics. We put a high-resistivity mirror-polished silicon (Si) plate at the aperture of the circular horn antenna. The complex refractive index of the Si plate measured at 60 GHz was $3.409 - j0.000$. The thickness of the plate was adjusted to be $440 \mu\text{m}$ in order to ensure maximum reflection. Fig. 8 shows reconstructed images obtained with and without the Si plate. Raw data sets for the images were obtained under the same experimental conditions described above. The sample was patterned Al on a quartz substrate depicted in the inset of Fig. 8(a), which has the reverse pattern of the sample shown in Fig. 5(a). Fig. 8(a) is a plot of the intensity of the near-field signal $|\Delta S_{21}|$ as a function of the distance between the Si

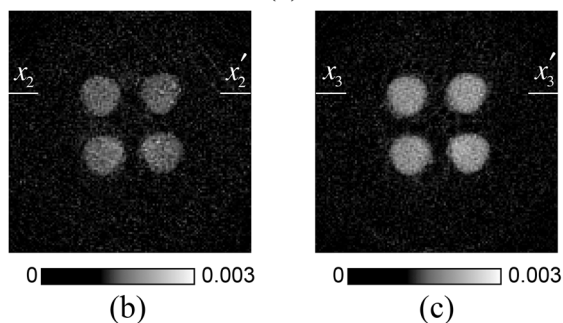
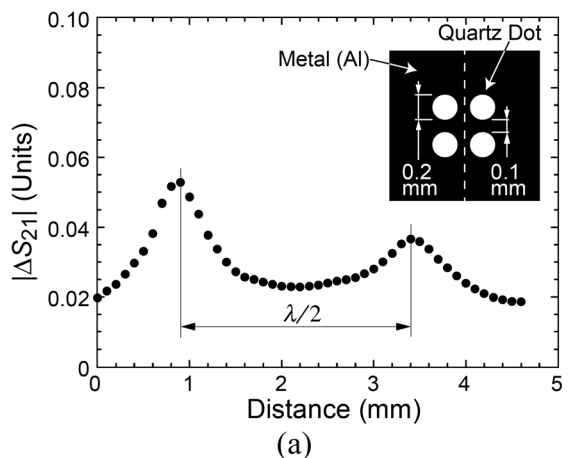


FIG. 8. Comparison of reconstructed intensity images obtained with and without a resonator in the illumination optics. (a) Intensity of the near-field signal $|\Delta S_{21}|$ when the distance between the Si plate and the corner reflector is varied. (b) Reconstructed intensity image without the resonator. (c) Reconstructed intensity image with the resonator.

plate and the corner reflector with the probe tip positioned above the center of the sample, as depicted by the dotted line in the inset. This is the relative distance to the point of closest approach of the Si plate to the reflector. This result indicates that this configuration works as a resonator. Data acquisition for the images was performed at the distance giving the maximum signal intensity in Fig. 8(a). As shown in the intensity images in Figs. 8(b) and 8(c) (see also Fig. 9), by incorporating this resonant structure in the illumination optics, the image intensity corresponding to the quartz dot improves by ~ 2 times (6.0 dB). Since the image intensity is proportional to the signal intensity, this result demonstrates that the intensity of the near-field signal is enhanced by more than 10 times (20 dB) using a knife blade probe compared with an equivalent metal tip probe. Because the images in Figs. 8(b) and 8(c) were reconstructed in order to set the image intensity and phase corresponding to Al to zero, the phase sign corresponding to the quartz dots in the phase images should change compared with that of the metal dots in Fig. 7(d). Although the reconstructed phase images for Figs. 8(b) and 8(c) are not shown, we confirmed this change of the phase sign (from negative to positive) in the phase images.

Fig. 9 shows one-dimensional intensity profiles along the line $x_1 - x'_1$ in Fig. 7(c), $x_2 - x'_2$ in Fig. 8(b), and $x_3 - x'_3$ in Fig. 8(c). They are smoothed profiles of the original ones after reducing noise. These profiles show that the image intensities at the edges of the Al dots ($x_1 - x'_1$) are enhanced and vary steeply while those of the quartz dots ($x_2 - x'_2$ and $x_3 - x'_3$) change gradually, i.e., the edges of the quartz dots become indistinct. The interaction between the probe tip and the samples can be treated quasi-statically. When the probe tip is scanned near the periphery of a metal (Al) dot, because most of the one-dimensional probe tip sees a dielectric (quartz), the electric field beneath the tip is concentrated at the metal edge, leading to an enhancement of the near-field signal, whereas in the case of a dielectric (quartz) dot surrounded by metal, the electric field coming from the probe tip terminates at the surrounding metal rather than the dielectric. This is a possible reason for this difference in the intensity profiles, which would not be observed using point-like metal tip probes.

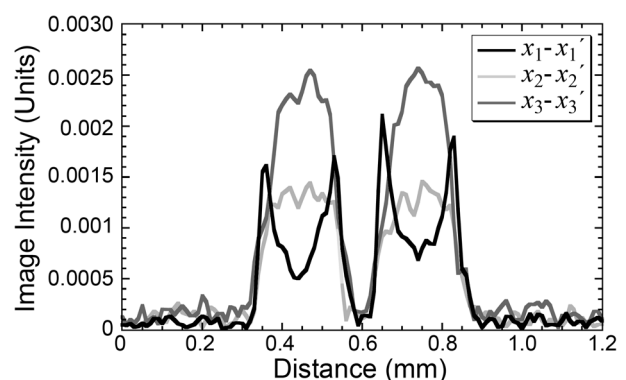


FIG. 9. One-dimensional intensity profiles along the line $x_1 - x'_1$ in Fig. 7(c), $x_2 - x'_2$ in Fig. 8(b), and $x_3 - x'_3$ in Fig. 8(c).

IV. CONCLUSIONS

A novel type of apertureless near-field microscopy using a knife blade as a scanning probe was proposed and investigated. Experiments performed at 60 GHz ($\lambda = 5$ mm) showed that the intensity of the near-field signal improves by ~ 6 times (15.6 dB) using a knife blade probe compared with an equivalent metal tip probe and that 2-D millimeter-wave images with subwavelength spatial resolution can be successfully reconstructed by adopting a scanning method and an image reconstruction algorithm based on computerized tomography. Further enhancement of the signal intensity was demonstrated by using a knife blade probe as a reflector for an open resonator in the illumination optics. In higher frequency regions, such as the terahertz and infrared regions, this enhancement is likely to be greater because of the higher quality factor of the resonator due to smaller diffraction losses. The format of the apertureless near-field microscopy investigated here should enable samples to be observed with higher sensitivity than that achieved using a metal tip and should reduce the measurement times required to record near-field images.

ACKNOWLEDGMENTS

This work was supported in part by a Grant-In-Aid for Scientific Research, No. 22360162 from the Japan Society for the Promotion of Science (JSPS).

- ¹B. T. Rosner and D. W. van der Weide, *Rev. Sci. Instrum.* **73**, 2505 (2002).
- ²F. Keilmann, D. W. van der Weide, T. Eickelkamp, R. Mertz, and D. Stöckle, *Opt. Commun.* **129**, 15 (1996).
- ³B. Knoll, F. Keilmann, A. Kramer, and G. Guckenberger, *Appl. Phys. Lett.* **70**, 2667 (1997).
- ⁴Y. Gao, A. Lauer, Q. Ren, and I. Wolff, *IEEE Trans. Microwave Theory Tech.* **46**, 1694 (1998).
- ⁵R. Kantor and I. V. Shvets, *IEEE Trans. Microwave Theory Tech.* **51**, 2228 (2003).
- ⁶M. Tabib-Azar and Y. Wang, *IEEE Trans. Microwave Theory Tech.* **52**, 971 (2004).
- ⁷A. Imtiaz, M. Pollak, S. M. Anlage, J. D. Barry, and J. Melngailis, *J. Appl. Phys.* **97**, 044302 (2005).
- ⁸A. Karbassi, C. A. Paulson, A. B. Kozyrev, M. Banerjee, Y. Wang, and D. W. van der Weide, *Appl. Phys. Lett.* **89**, 153113 (2006).
- ⁹A. Imtiaz, M. Pollak, S. M. Anlage, J. D. Barry, and J. Melngailis, *Appl. Phys. Lett.* **90**, 143106 (2007).
- ¹⁰M. Tabib-Azar, N. S. Shoemaker, and S. Harris, *Meas. Sci. Technol.* **4**, 583 (1993).
- ¹¹M. Tabib-Azar, D.-P. Su, A. Pohar, S. R. LeClair, and G. Ponchak, *Rev. Sci. Instrum.* **70**, 1725 (1999).
- ¹²W. Charles Symons III, K. W. Whites, and R. A. Lodder, *IEEE Trans. Microwave Theory Tech.* **51**, 91 (2003).
- ¹³N. S. Greeney and J. A. Scales, *Appl. Phys. Lett.* **91**, 222909 (2007).
- ¹⁴M. D. Weiss, B. Zadler, S. Schafer, and J. Scales, *J. Appl. Phys.* **106**, 044912 (2009).
- ¹⁵M. Golosovsky, A. Galkin, and D. Davidov, *IEEE Trans. Microwave Theory Tech.* **44**, 1390 (1998).
- ¹⁶T. Nozokido, J. Bae, and K. Mizuno, *IEEE Trans. Microwave Theory Tech.* **49**, 491 (2001).
- ¹⁷T. Nozokido, R. Iibuchi, H. Kudo, J. Bae, and K. Mizuno, *Rev. Sci. Instrum.* **76**, 033702 (2005).
- ¹⁸T. Nozokido, M. Noto, and T. Murai, *IEEE Microw. Wirel. Compon. Lett.* **19**, 638 (2009).
- ¹⁹M. M. Awad and R. A. Cheville, *Appl. Phys. Lett.* **86**, 221107 (2005).
- ²⁰H. Merbold and T. Feurer, *J. Appl. Phys.* **107**, 033504 (2010).
- ²¹J. Liu, R. Mendis, D. M. Mittleman, and N. Sakoda, *Appl. Phys. Lett.* **100**, 031101 (2012).
- ²²R. Merz, F. Keilmann, R. J. Haug, and K. Ploog, *Phys. Rev. Lett.* **70**, 651 (1993).
- ²³F. Bueersgens, R. Kersting, and H.-T. Chen, *Appl. Phys. Lett.* **88**, 112115 (2006).
- ²⁴J.-B. Masson, M.-P. Sauviat, and G. Gallot, *Appl. Phys. Lett.* **89**, 153904 (2006).
- ²⁵B. Knoll and F. Keilmann, *Nature* **399**, 134 (1999).
- ²⁶B. Knoll and F. Keilmann, *Opt. Commun.* **182**, 321 (2000).
- ²⁷B. Knoll and F. Keilmann, *Appl. Phys. Lett.* **77**, 3980 (2000).
- ²⁸H.-T. Chen, R. Kersting, and G. C. Cho, *Appl. Phys. Lett.* **83**, 3009 (2003).
- ²⁹P. C. M. Planken and N. C. J. van der Valk, *Opt. Lett.* **29**, 2306 (2004).
- ³⁰H.-T. Chen, S. Kraatz, G. C. Cho, and R. Kersting, *Phys. Rev. Lett.* **93**, 267401 (2004).
- ³¹H.-G. von Ribbeck, M. Brehm, D. W. van der Weide, S. Winneri, O. Drachenko, M. Helm, and F. Keilmann, *Opt. Express* **16**, 3430 (2008).
- ³²V. Astley, H. Zhan, R. Mendis, and D. M. Mittleman, *J. Appl. Phys.* **105**, 113117 (2009).
- ³³R. Adam, L. Chusseau, T. Grosjean, A. Penarier, J.-P. Guillet, and D. Charraut, *J. Appl. Phys.* **106**, 073107 (2009).
- ³⁴Y. Kajihara, K. Kosaka, and S. Komiyama, *Rev. Sci. Instrum.* **81**, 033706 (2010).
- ³⁵K. Moon, E. Jung, M. Lim, Y. Do, and H. Han, *IEEE Trans. Terahertz Sci. Technol.* **1**, 164 (2011).
- ³⁶A. C. Kak and M. Slaney, *Principles of Computerized Tomographic Imaging* (IEEE, New York, 1988), Chap. 3.
- ³⁷W. L. Stutzman and G. A. Thiele, *Antenna Theory and Design*, 2nd ed. (Wiley, Hoboken, 1998), Chaps. 5 and 6.